Hindawi
Advances in Materials Science and Engineering
Volume 2022, Article ID 8390315, 9 pages
https://doi.org/10.1155/2022/8390315

Research Article

Continuously Varying Thickness Interference Bandpass Filter for the Visible Spectral Range: Using Ion Beam Sputter Deposition

Anayat Ullah,[1] **Muhammad Rizwan Amirzada**,[2] **M. D. Rifat Jahan**,[3] **and Yousuf Khan**[1]

[1]*Department of Electronic Engineering, Balochistan University of Information Technology Engineering and Management Sciences (BUITEMS), Takatu Campus, Airport Road, Baleli, Quetta 87300, Pakistan*
[2]*Faculty of Engineering and Computer Science, National University of Modern Languages, Islamabad 44000, Pakistan*
[3]*Department of Electronics and Telecommunication Engineering, Rajshahi University of Engineering & Technology (RUET), Rajshahi 6204, Bangladesh*

Correspondence should be addressed to M. D. Rifat Jahan; 1604048@student.ruet.ac.bd

Received 27 June 2022; Revised 20 September 2022; Accepted 25 October 2022; Published 12 November 2022

Academic Editor: Alessandro Martucci

Optical bandpass filters, used to restrict certain wavelengths while allowing other wavelengths to pass, are a common element in many optical devices, such as spectroscopic sensors and hyperspectral imagers. Such filters can be implemented using interference filters, which operate on the principle of constructive and destructive interference. In this work, an interference bandpass filter with continuously varying thicknesses of the constituent films is designed and fabricated for the visible spectral range. Niobium pentoxide and silicon dioxide are used as the filter materials due to the high refractive index contrast between them, resulting in a smaller number of required material films. Ion beam sputter deposition is used as the deposition method due to its ability to produce accurate thickness high optical quality films. The fabricated filter has a transmission band of 130 nm, i.e., 470–600 nm, and can block wavelengths as low as 300 nm and as high as 1080 nm, which is sufficient for use with silicon-based detectors in the visible spectral range. The maximum and minimum transmission inside the transmission band is 96% and 71%, respectively, with an average transmission of 88%. The transmission outside the transmission band is less than 1.6%.

1. Introduction

In many optical applications, such as optical micro-electro mechanical systems (MEMS), it is required that a certain band of wavelengths be allowed to pass while restricting other wavelengths [1, 2]. For example, silicon (Si)-based charge-coupled devices (CCDs) can detect wavelengths from 300–1100 nm. To restrict wavelengths outside the visible range (400–700 nm) for optical applications, a bandpass filter is required. Hyperspectral imagers (used for mineral, vegetation, or flood detection when onboard satellites or UAVs) and spectroscopic sensors (used for on-site meat and milk quality control and noninvasive blood testing in the form of mobile sensors) can be implemented using Si-based detectors and Fabry–Pérot (FP) filters [3–5]. FP filters are formed by two highly reflecting mirrors, usually distributed Bragg reflectors (DBRs) consisting of alternating high and low refractive index material pairs, with a central cavity between them. The output transmission wavelength of a FP filter depends on the thickness of the central cavity and can be varied by varying the cavity thickness within a stopband, strong reflection band, formed by the DBRs. The stopband of the DBRs is governed by the refractive index contrast of the materials used, as well as their optical thicknesses (physical thickness × refractive index). The stopband is formed around a central wavelength, which is four times the optical thickness of the films. The DBR materials are therefore a quarter-wave thick of the central wavelength. The stopband of a DBR is usually 80 to 180 nm in the visible spectral range, depending on the index contrast of the material pair and

their thickness. Combining a DBR-based FP filter with a Si-based detector, for spectroscopic and hyperspectral imaging applications, therefore requires a bandpass filter to restrict wavelengths outside the DBR stopband.

A bandpass filter will ideally be 100% transmitting within the DBR stopband, while 100% rejecting otherwise. Color filters that work by selective transmission and absorption of light are not flexible enough to cater for the specific transmission and rejection bands required. Interference bandpass filters that work by transmission and reflection of light, on the other hand, can meet these specific design requirements [6].

A basic interference filter consists of quarter-wave thick alternating high and low refractive index material pairs. An interference bandpass filter can be formed using two edge filters, which are defined by a transmission edge and reject all wavelengths beyond it. Combining a shortpass (allowing shorter wavelengths to pass) and a longpass (allowing longer wavelengths to pass) edge filter forms a bandpass filter [7]. In such a design, the most frequent problem is the interference of the edge filters with each other, causing multiple reflection peaks called fringes at the two extremes of the transmission band. These fringes are further enhanced as the number of material pair increases, which is needed to steepen the slope of the band edges and/or extending the rejection band. One way to reduce these fringes, to some extent, is by adding half-quarter-wave thick matching layers. Adding a half-quarter-wave thick film of the high refractive index material before and after the longpass filter stack results in decreased ripples inside the pass region [8]. On the other hand, for a shortpass filter stack, fringes are reduced by adding a half-quarter-wave thick film of the low refractive index material. However, to form a large rejection band, multiple long- and shortpass filters are combined. This further enhances the fringes inside the transmission band. Therefore, an alternative approach needs to be employed.

Using computer-aided design techniques, it is now possible to design bandpass filters with almost any desired optical spectra [9–11]. However, such a design can consist of tens of hundreds of layers with continuously varying thicknesses. The challenge is to fabricate such designs with extremely accurate thicknesses and high optical purity.

Most optical coatings are fabricated using different variants of chemical vapor deposition (CVD), e.g., plasma-enhanced CVD or *e*-beam and thermal evaporation [12]. However, materials deposited with these technologies have poor optical quality. Evaporated films are generally porous resulting in filters with poor humidity [7, 11]. On the other hand, CVD processes lack in-situ measurement and control of deposition rates and film stoichiometry resulting in variant layer thicknesses and refractive indices compared to the desired values. This results in a difference between the designed and measured filter spectra. Ion beam sputter deposition (IBSD), on the other hand, provides a high control on deposition rates and film stoichiometry, resulting in very accurate thickness high-quality films [13].

Furthermore, using materials with a high refractive index contrast between them as the high and low refractive index material pairs will result in reducing the total number of pairs required in the filter design. Two such materials, having a high refractive index contrast between them [7, 14], are niobium pentoxide (Nb2O5) and silicon dioxide (SiO2).

Combining computer-aided design techniques with IBSD Nb_2O_5 and SiO_2 films will result in high optical quality bandpass filters, meeting specific transmission and rejection band requirements.

1.1. Theory. Several different design techniques can be employed to simulate the required spectrum [15, 16]. These methods can broadly be categorized as refinement and synthesis methods. In refinement, a starting design is provided, which has a spectrum that is a close approximation of the desired spectrum; whereas, in synthesis, no such design is defined. Given a suitable starting design, the refinement method gradually modifies the construction parameters to minimize a merit function defining the quality of the design [17, 18]. The merit function is determined by defining targets at a single or a range of wavelengths. However, refinement techniques are limited in their design capabilities, which makes the need of a suitable initial design even more critical. It is challenging to guess not only the initial number of layers but also the initial overall thickness of the starting design, which makes it difficult to reach closer to the desired spectra. Synthesis methods overcome this problem by employing a comprehensive search method. Two most common synthesis design methods are the Fourier transform method and the needle synthesis method. Both methods are explained below.

(1) In the Fourier transform synthesis method, the refractive indices of the layers are varied to alter the amplitude relationship among the reflected waves during the optimization process. This method generates coatings with a continuously varying refractive index profile which can be transformed into two-material multilayer systems using an extra step. The latter is usually subjected to further refinement, see references [18, 19].

(2) In the needle synthesis method, the thicknesses are varied to alter the phase relationship among the reflected waves during the optimization process. This method generates two-material multilayer systems based on actual dispersive materials. This method uses a merit function to add thin layers (called needles) at optimal positions in the filter and then adjusts their thickness by refinement techniques, see reference [17].

2. Materials and Methods

The deposition process of Nb_2O_5 and SiO_2 using IBSD is optimized first for high deposition rate and low absorption. The optical constants for the filter design are then obtained using post-deposition ellipsometry measurements of films optimized for deposition. A variable angle spectroscopic ellipsometer is used for this purpose. The ellipsometry measurements were performed at three different angles near Brewster's angle. The Cauchy equation is used to

parameterize the SiO_2 films, while the Tauc–Lorentz oscillator model is used for the Nb_2O_5 films. Table 1 gives a comparison of different parameters between the films deposited by Nb_2O_5/SiO_2 and Ta_2O_5/ZrO_2.

SiO_2 has a large bandgap; therefore, the resonant wavelength lies in the ultraviolet (UV) wavelength range. A strong absorption is hence observed in this region, where the refractive index first increases and then decreases with decreasing wavelength. While in the visible wavelength, the refractive index decreases with increasing wavelength [20]. The Cauchy equation can easily be used to model the behavior of the refractive index of SiO_2 at visible wavelengths, which is essentially a curve (equation (1)).

$$n(\lambda) = A_n + \frac{B_n}{\lambda^2} + \frac{C_n}{\lambda^4}, \tag{1}$$

where A_n, B_n, and C_n are called the Cauchy coefficients. A_n is a constant value and sets a base line for the curve, B_n introduces a curvature to this line at lower wavelengths, while C_n adds more curvature to the equation. To cater for the absorption near the UV range, the Cauchy equation is combined with the Urbach absorption (equation (2)).

$$k(\lambda) = A_k e^{B_k\left(1.24\left(\frac{1}{\lambda} - \frac{1}{C_k}\right)\right)}, \tag{2}$$

where A_k is the absorption amplitude, B_k is the broadening, and C_k is the absorption band edge.

Nb_2O_5, on the other hand, has significant absorption in the visible spectrum near the UV range [20]. The Cauchy equation is insufficient to explain this behavior. Therefore, the Tauc–Lorentz oscillator model is used in this case. The Tauc–Lorentz oscillator model requires five terms to define the imaginary part (ε_2) of the complex dielectric function $(\tilde{\varepsilon})E_g$, i.e., the center energy (E_c), amplitude (A), broadening (B_r), bandgap energy (E_g), and ε_1-offset. The real part of the complex dielectric function and consequently the refractive index (n) and extinction coefficient (k) are derived from the Kramer–Kronig relationship as given in equation (3) [21].

$$\tilde{\varepsilon} = \varepsilon_1 + i\varepsilon_2 + \tilde{n}^2 = (n + ik)^2. \tag{3}$$

The starting parameters for both models are shown in Tables 2 and 3, respectively.

The mean square error values in the parameterizing of the optical constants is recorded to be less than 5 in all cases. The optical properties thus obtained are used to design the bandpass filter.

A comprehensive design technique comprising of manual, synthesis, and refinement methods is employed in this work. After first manually adjusting the values to bring them closer to the desired profile, the needle synthesis method was used for the design which was stopped after visually inspecting results to be close to the desired profile. A final refinement step was employed to increase the smoothness of the filter profile. However, in all the steps employed, only the phase relationship of the waves is altered by optimizing the layer thicknesses, while the refractive indices of the materials are fixed (amplitude of the waves is not altered).

An open-source software, OpenFilters [8, 17], is used in this work to design and optimize the required bandpass filter. The design targets for the bandpass filter are shown in Table 4.

The filter is required to have 90% transmission in the 475 – 610 nm wavelength range. This wavelength range is carefully selected to achieve one mode transmission while tuning a Fabry–Pérot filter having its output transmission wavelength centered at 525 nm. First, an initial design is synthesized manually, combining one longpass and three shortpass filters. The fringes inside the transmission band are minimized using half-quarter-wave matching layers. After an initial refinement step, the needle optimization technique is employed to improve the performance. However, the needle optimization is restricted in the total number of needles allowed to keep the design within economic limits. A final refinement step is employed to allow the needles to grow to their optimal thickness.

Depositions are performed using an IBSD system *IonSys* 1000 from Roth & Rau on a borosilicate glass substrate. The deposition assembly is equipped with two electron cyclotron resonance plasma sources. The setup has a cryogenically pumped vacuum chamber which can achieve a typical base pressure of 1.7×10^{-7} mbar. A primary ion source sputters 99.99% pure Si and 99.95% pure niobium (Nb) targets with argon ions (Ar^+), referred to as the sputtering gas ions, at a target incidence angle (angle between ion beam and target normal) of 60°, while maintaining a constant ion flux. The substrate is placed on a circular substrate holder in front of the target at a distance of 30 cm such that it is in line with the target normal. The substrate holder is tilted at a 45° angle with respect to the target normal and is rotating at 60 rpm. Oxygen is introduced into the chamber to form the oxide films using a second ion source, which can also be utilized to ionize the introduced oxygen. Ionized oxygen is more reactive than molecular oxygen and the required ionized oxygen flow for full oxidation of the sputtered material is comparatively lower [3, 23]. The whole assembly is enclosed inside a 450-liter chamber. The deposition process is optimized for fast deposition and low absorption. The deposition parameters are as given in Table 5.

The transmission spectrum of the deposited filter is measured using an optical spectrum analyzer *AQ6375* from YOKOGAWA in combination with a microscope. Measurements are made in the 300–1100 nm wavelength range with a resolution of 0.1 nm.

3. Results and Discussion

The refractive index and extinction coefficient of the films optimized for deposition, achieved using ellipsometry, are shown in Figures 1 and 2. Both Nb_2O_5 and SiO_2 show near zero absorption at visible wavelengths.

The filter designed and optimized using these optical properties has a total of 79 layers with a total thickness of 8.437 μm. Table 6 shows the optimized film thicknesses of the filter materials, while Figure 3 shows the refractive index change along the depth of the filter.

Table 1: Comparison of different parameters of a state-of-the-art optical filter with this work.

Author	Central wavelength (nm)	Stopband (nm)	Stopband (nm)	Materials used	No. of layers	Total thickness (μm)	Fabrication method	Min Tx in passband (%)	Max Tx in stopband (%)
Achieved results	550	130	300–1100	Nb_2O_5/ SiO_2	79	8.4	Dual ion beam sputter deposition	71	1.6
Burns et al.	399	32	200–1100	Ta_2O_5/ ZrO_2	227	23.4	Enhanced optical sputtering system	80	0.1

Table 2: Starting parameters of the Cauchy equation for SiO_2 films [22].

A_n	1.4
B_n	0
C_n	0
A_k	0
B_k	1.5
C_k	400 nm

Table 3: Starting parameters of the Tauc–Lorentz oscillator for Nb_2O_5 films [22].

E_c	4.6 eV
A	208
E_g	3.4 eV
ε_1-offset	1.9 eV
B_r	2.1 eV

Table 4: Design targets for the bandpass filter [22].

Wavelength (nm)	Transmission (%)	Tolerance
300 – 470	0	0.001
475 – 610	90	0.001
615 – 1100	0	0.001

Table 5: Deposition parameters for Nb_2O_5 and SiO_2 films [22].

	Nb_2O_5	SiO_2
Target material	99.95% pure Nb	99.99% pure S
Sputtering gas	Ar^+	Ar^+
Sputtering gas flow	4 sccm	4 sccm
Sputtering gas ion energy	800 eV	800 eV
Sputtering gas ion flux	75 mA	75 mA
Sputtering angle	60°	60°
Substrate tilt angle	45°	45°
Substrate rotation	60 rpm	60 rpm
Reactive gas	O^+	O^+
Reactive gas flow	10 sccm	10 sccm
Reactive gas ion energy	200 eV	200 eV
Reactive gas ion flux	~2.5 mA	~2.5 mA

The designed (theoretical) and measured (experimental) spectra of the bandpass filter are shown in Figure 4.

The fabricated filter has a transmission band of passband of 130 nm, i.e., 470–600 nm. The average transmission inside this transmission band is 88% with a maximum and minimum transmission of 96% and 71%, respectively (Figure 5(a)). The maximum transmission outside the transmission band is less than 1.6%, Figure 5(b). The filter has a broad rejection region, i.e., 300–470 nm and 600–1080 nm.

A shift in the measured spectrum is observed compared to the designed spectrum with increasing wavelength, Figure 4. This is due to the fact that the Cauchy equation used to obtain the optical constants of SiO_2 flattens at longer wavelengths and cannot fit the index at those wavelengths correctly. The error in the refractive index translates to errors in thickness calculation which ultimately translates into a shift in the spectrum. The Sellmeier equation [24] is a better alternative to the Cauchy equation, since it not only accounts for electronic oscillations at shorter wavelengths but also for atomic oscillations at longer wavelengths. The measured transmission spectrum shows a fringe at the higher wavelength extreme of the passband, contrary to the designed spectrum. This fringe appears because filter optimization is performed by including the substrate/air interface reflections into account. However, in practice, due to the substrate surface roughness, reflections from the substrate/air interface are minimized to zero and do not take part in interference. These reflections must hence be ignored. The theoretical transmission spectrum of the designed filter, excluding the substrate reflections, shows a similar fringe at the higher wavelength extreme of the passband, Figure 6.

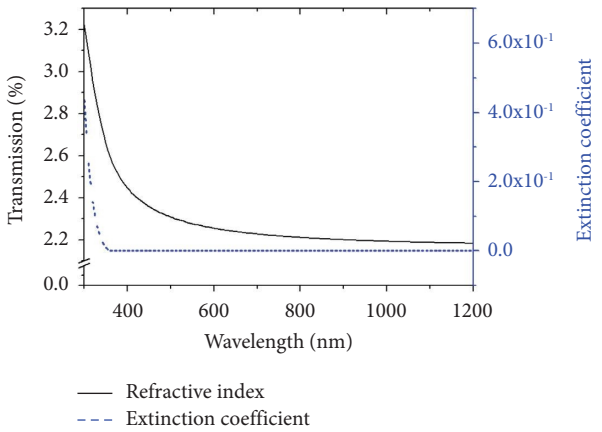

Figure 1: Calculated optical properties of sputtered Nb_2O_5 using the Tauc–Lorentz oscillator model [22].

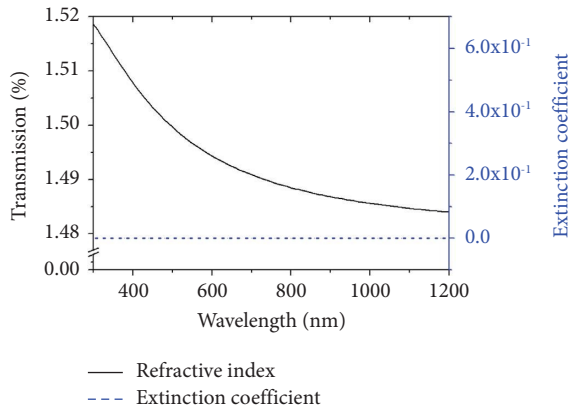

Figure 2: Calculated optical properties of sputtered SiO_2 using the Cauchy equation [22].

Table 6: Material thicknesses (Th.) of the quarter-wave bandpass filter design [22].

Layer no.	Material	Thickness (nm)
1	Nb_2O_5	10.4
2	SiO_2	238.6
3	Nb_2O_5	33.8
4	SiO_2	84.6
5	Nb_2O_5	24.1
6	SiO_2	64.7
7	Nb_2O_5	43.5
8	SiO_2	87.5
9	Nb_2O_5	41.9
10	SiO_2	53.4
11	Nb_2O_5	34
12	SiO_2	83.4
13	Nb_2O_5	45
14	SiO_2	81.2
15	Nb_2O_5	33.5
16	SiO_2	60.6
17	Nb_2O_5	40.3
18	SiO_2	84.2
19	Nb_2O_5	36.4
20	SiO_2	70
21	Nb_2O_5	128.6
22	SiO_2	95.9

Table 6: Continued.

Layer no.	Material	Thickness (nm)
23	Nb_2O_5	62.7
24	SiO_2	147.8
25	Nb_2O_5	80.1
26	SiO_2	97.2
27	Nb_2O_5	67
28	SiO_2	149.6
29	Nb_2O_5	69
30	SiO_2	101.5
31	Nb_2O_5	76.3
32	SiO_2	142.6
33	Nb_2O_5	65
34	SiO_2	105.6
35	Nb_2O_5	83.7
36	SiO_2	129.2
37	Nb_2O_5	71.9
38	SiO_2	116.4
39	Nb_2O_5	99
40	SiO_2	137.7
41	Nb_2O_5	112.3
42	SiO_2	114.2
43	Nb_2O_5	89.1
44	SiO_2	141.9
45	Nb_2O_5	70.3
46	SiO_2	191.3
47	Nb_2O_5	116.3
48	SiO_2	155.2
49	Nb_2O_5	49
50	SiO_2	179.3
51	Nb_2O_5	65.1
52	SiO_2	185.4
53	Nb_2O_5	89.3
54	SiO_2	165.6
55	Nb_2O_5	57.6
56	SiO_2	149
57	Nb_2O_5	97.4
58	SiO_2	191.8
59	Nb_2O_5	103
60	SiO_2	142.2
61	Nb_2O_5	118
62	SiO_2	180.4
63	Nb_2O_5	94.1
64	SiO_2	188.5
65	Nb_2O_5	122.5
66	SiO_2	148
67	Nb_2O_5	116.6
68	SiO_2	197.9
69	Nb_2O_5	99.2
70	SiO_2	140.1
71	Nb_2O_5	103.2
72	SiO_2	196.7
73	Nb_2O_5	95.1
74	SiO_2	165.5
75	Nb_2O_5	150.7
76	SiO_2	199
77	Nb_2O_5	125.1
78	SiO_2	143.7
79	Nb_2O_5	109

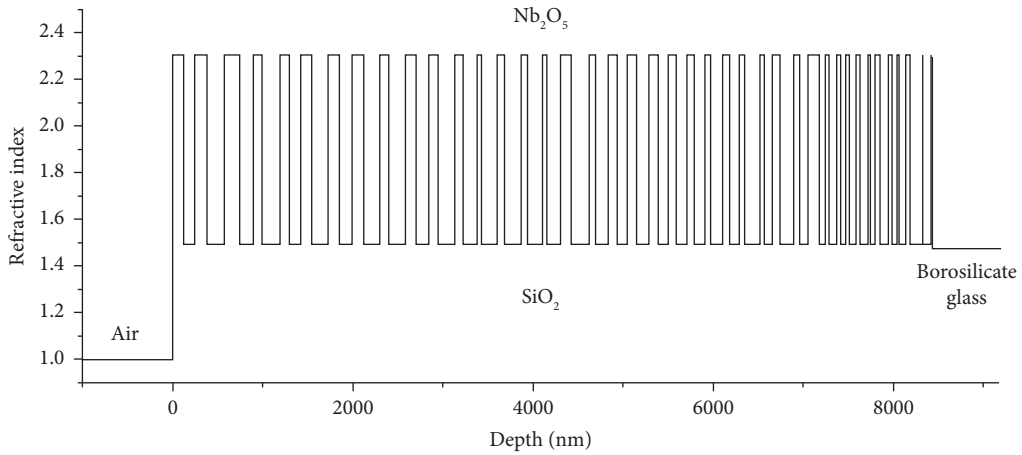

Figure 3: Change in the refractive index along the depth of the bandpass filter with nonquarter-wave design, showing the layer design structure, i.e., the thicknesses of Nb_2O_5 and SiO_2 along the depth of the filter [22].

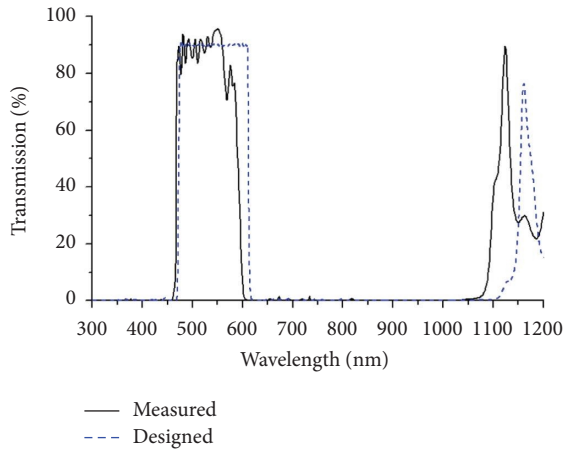

Figure 4: Designed (theoretical) and measured (experimental) transmission spectra of the bandpass filter [22].

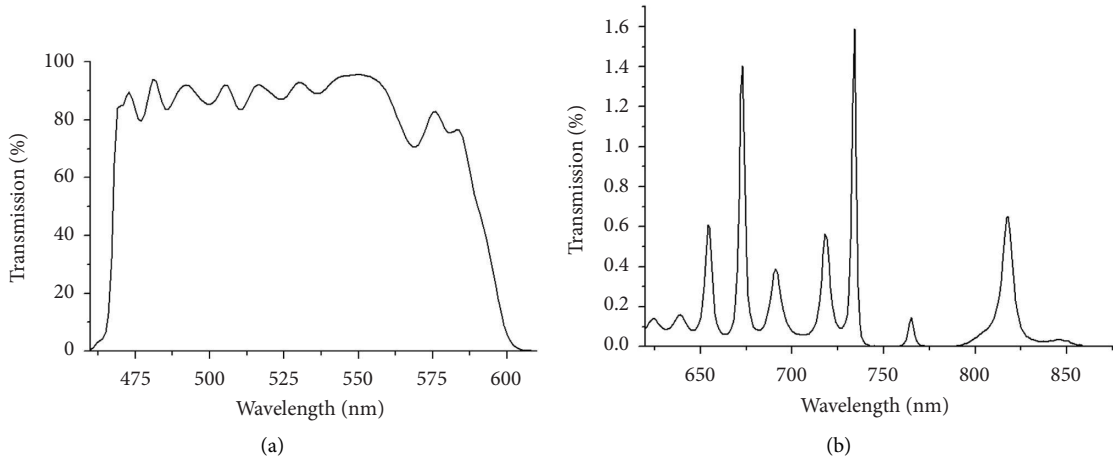

Figure 5: A zoom in at the measured transmission of the bandpass filter. (a) The average transmission inside the passband is 88%. (b) Maximum transmission outside the passband is a mere 1.6% [22].

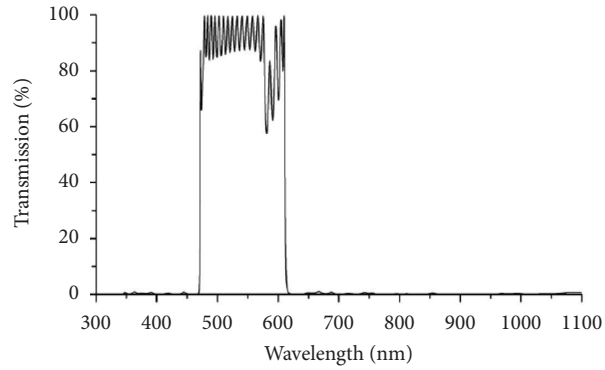

Figure 6: Transmission spectrum of the designed bandpass filter excluding the substrate reflections [22].

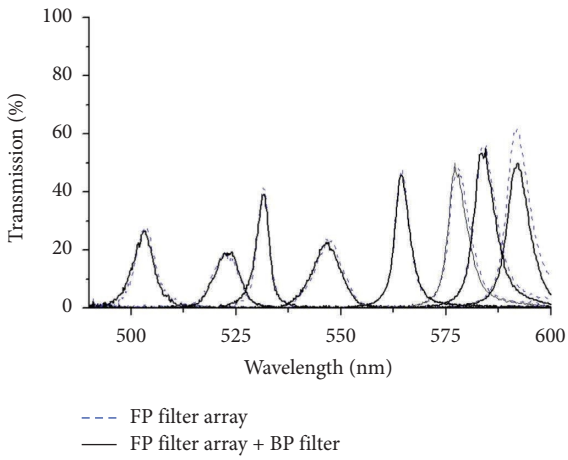

Figure 7: Experimental transmission spectra of the Fabry–Pérot filter array with distinct cavity heights and its combined spectra with the fabricated bandpass filter [22].

Hence, the filter design must be optimized without including the substrate/air interface reflections to achieve optimum results.

Figure 7 shows the combined spectrum of the bandpass filter with the Fabry–Pérot filter array having distinct cavity heights, as reported earlier in reference [24]. The loss in transmission is very low except for the transmission lines near the higher wavelength edge of the filter transmission band (~600 nm), where it is being suppressed by the slope of the filter transmission edge.

4. Conclusions

An interference bandpass filter with continuously varying thicknesses of the high and low refractive index material pairs has been designed and fabricated in this work. A comprehensive design technique comprising manual and computer-aided design methods is employed for this purpose. The needle optimization technique is also utilized in the filter design, among others. A 79-layered (total thickness = 8.437 μm) Nb_2O_5/SiO_2 filter is designed and fabricated using IBSD. The filter has a transmission band of 130 nm and can block wavelengths as low as 300 nm and as high as 1080 nm, which is sufficient for use with Si-based detectors in the visible range. The filter has a high average transmission of 88% inside the transmission band (with a maximum and minimum transmission of 96% and 71%, respectively), while the transmission outside the transmission band is very low (less than 1.6%). The transmission inside the transmission band can further be improved by ignoring the reflections from the substrate/air interface during the filter design and optimization process since in practice light is scattered from this interface due to the surface roughness of the glass substrate and does not contribute to light interference.

Data Availability

The data used to support the findings of this study are available from the corresponding author upon request.

Conflicts of Interest

The authors declare that they have no known conflicts of interest.

Acknowledgments

The authors wish to thank the technical staff and all the colleagues at the Institute of Nanostructures and Analytics (INA), Germany, for their technical support and discussions and for providing facilities and necessary support in conducting experiments.

References

[1] M. R. Amirzada, Q. Li, and H. Hillmer, "Development of optical MEMS-based micromirror arrays on a flexible substrate for curvilinear surfaces," *Optical and Quantum Electronics*, vol. 53, no. 5, pp. 210–10, 2021.

[2] H. Hillmer, B. Al-Qargholi, M. M. Khan, M. S. Q. Iskhandar, H. Wilke, and A. Tatzel, "Optical MEMS based micromirror arrays: fabrication, characterization and potential applications in smart active windows," in *Proceedings of the 2019 International Conference on Optical MEMS and Nanophotonics (OMN)*, Daejeon, Korea, August 2019.

[3] D. B. Todorov, "Development of Hybrid UV VCSEL with Organic Active Material and Dielectric DBR Mirrors for Medical , Sensoric and Data Storage Applications Erklärung," 2008, https://d-nb.info/1000169421/34.

[4] H. Saari, V. V. Aallos, A. Akujarvi et al., "Novel miniaturized hyperspectral sensor for UAV and space applications," *SPIE Proceedings*, vol. 7474, no. September, Article ID 74741M, 2009.

[5] J. L. Ferrari, K. D. O. Lima, and R. R. Gonçalves, "Refractive indexes and spectroscopic properties to design Er3+-doped SiO2-Ta2O5Films as multifunctional planar waveguide platforms for optical sensors and amplifiers," *ACS Omega*, vol. 6, no. 13, pp. 8784–8796, 2021.

[6] Y. Zhang, "Design and realization of multispectral bandpass filters for space applications," *Critical Reviews in Solid State and Materials Sciences*, vol. 6, no. 05, pp. 8784–8796, 2021.

[7] R. Gadhwal, P. Kaushik, and A. Devi, "A review on 1D photonic crystal based reflective optical limiters," *Critical Reviews in Solid State and Materials Sciences*, vol. 0, no. 0, pp. 1–19, 2022.

[8] A. McClung, S. Samudrala, M. Torfeh, M. Mansouree, and A. Arbabi, "Snapshot spectral imaging with parallel metasystems," *Science Advances*, vol. 6, no. 38, pp. eabc7646–9, 2020.

[9] T. S. Ftlms, "97 Computer Design of Optical Coatings ∗ ," *Thin Solid Films*, vol. 163, pp. 97–110, 1988.

[10] B. T. Sullivan, J. Dobrowolski, G. Clarke et al., "Manufacture of complex optical multilayer filters using an automated deposition system," *Vacuum*, vol. 51, no. 4, pp. 647–654, 1998.

[11] C. Goury, U. Brauneck, V. Naulin et al., "Design and realization of multispectral bandpass filters for space applications," in *Proceedings of the International Conference on Space Optics — ICSO 2018*, vol. 11180, p. 297, Crete, Greece, October 2018.

[12] M. R. Amirzada, A. Tatzel, V. Viereck, and H. Hillmer, "Surface roughness analysis of SiO2 for PECVD, PVD and IBD on different substrates," *Applied Nanoscience*, vol. 6, no. 2, pp. 215–222, 2016.

[13] M. Schneider, S. Bruns, K. Galonska, M. Vergöhl, P. Henning, and T. Melzig, "Sputtering Platform for Double-Sided Precision Optical Coatings," in *Proceedings of the SPIE 1200*, p. 40, San Francisco, CA, USA, March 2022.

[14] F. Richter, H. Kupfer, P. Schlott, T. Gessner, and C. Kaufmann, "Optical properties and mechanical stress in SiO2/Nb2O5 multilayers," *Thin Solid Films*, vol. 389, no. 1–2, pp. 278–283, 2001.

[15] M. K. Ehsan and D. Dahlhaus, "Statistical modeling of ISM data traffic in indoor environments for cognitive radio systems," in *Proceedings of the 2015 3rd Int2015 Third International Conference on Digital Information, Networking, and Wireless Communications (DINWC) 2015*, pp. 88–93, Manhattan, NY, USA, February 2015.

[16] M. K. Ehsan, "Performance analysis of the probabilistic models of ISM data traffic in cognitive radio enabled radio environments," *IEEE Access*, vol. 8, pp. 140–150, 2020.

[17] S. Larouche and L. Martinu, "OpenFilters: open-source software for the design, optimization, and synthesis of optical filters," *Applied Optics*, vol. 47, no. 13, pp. 219–230, 2008.

[18] M. Duris, D. Deubel, L. Bodiou, C. Vaudry, J. C. Keromnes, and J. Charrier, "Fabrication of Ge-ZnS multilayered optical filters for mid-infrared applications," *Thin Solid Films*, vol. 719, p. 138488, Article ID 138488, 2021.

[19] J. A. Dobrowolski and D. Lowe, "Optical thin film synthesis program based on the use of Fourier transforms," *Applied Optics*, vol. 17, no. 19, p. 3039, 1978.

[20] S. Bruns, C. Britze, M. Vergoehl, A. Feller, and S. Meining, "UV bandpass filters based on Ta2O5 and ZrO2 for solar observation," no," p. 61, June 2021.

[21] H. . Tompkins, *WVASE32 Software Training Manual*, J. A. Woollam Co. Inc, Lincoln, Nebraska.

[22] A. Ullah, *Optimization of the Mechanical and Optical Properties of Tunable Optical Sensor Arrays (TOSA) for a Nanospectrometer in the Visible and Near Infrared Spectral Range*Universität Kassel, Kassel, Germany, Print, 2015.

[23] N. F. Zubair, S. Jamil, S. Fatima, S. R. Khan, M. U. Khan, and M. R. S. A. Janjua, "Synthesis of needle like nano composite of rGO-Mn2O and their applications as photo-catalyst," *Chemical Physics Letters*, vol. 757, no. August, Article ID 137874, 2020.

[24] A. Ullah, H. Wilke, I. Memon et al., "Stress relaxation in dual ion beam sputtered Nb2O5 and SiO2 thin films: application in a Fabry-Pérot filter array with 3D nanoimprinted cavities," *Journal of Micromechanics and Microengineering*, vol. 25, no. 5, Article ID 055019, 2015.